

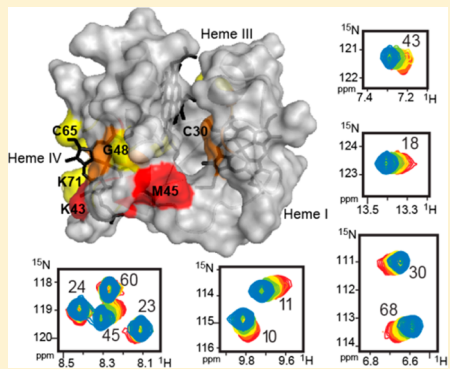
# Probing the Effect of Ionic Strength on the Functional Robustness of the Triheme Cytochrome PpcA from *Geobacter sulfurreducens*: A Contribution for Optimizing Biofuel Cell's Power Density

Joana M. Dantas,<sup>†</sup> Leonor Morgado,<sup>†</sup> Ana C. Marques, and Carlos A. Salgueiro\*

Requimte-CQFB, Departamento de Química, Faculdade de Ciências e Tecnologia, Universidade Nova de Lisboa, Campus Caparica, 2829-516 Caparica, Portugal

## S Supporting Information

**ABSTRACT:** The increase of conductivity of electrolytes favors the current production in microbial fuel cells (MFCs). Adaptation of cell cultures to higher ionic strength is a promising strategy to increase electricity production. The bacterium *Geobacter sulfurreducens* is considered a leading candidate for MFCs. Therefore, it is important to evaluate the impact of the ionic strength on the functional properties of key periplasmic proteins that warrants electron transfer to cell exterior. The effect of the ionic strength on the functional properties of triheme cytochrome PpcA, the most abundant periplasmic cytochrome in *G. sulfurreducens*, was investigated by NMR and potentiometric methods. The redox properties of heme IV are the most affected ones. Chemical shift perturbation measurements on the backbone NMR signals, at increasing ionic strength, also showed that the region close to heme IV is the most affected due to the large number of positively charged residues, which confer a highly positive electrostatic surface around this heme. The shielding of these positive charges at high ionic strength explain the observed decrease in the reduction potential of heme IV and shows that PpcA was designed to maintain its functional mechanistic features even at high ionic strength.



## INTRODUCTION

In the past decade, several studies have demonstrated that members of the *Geobacteraceae* family can transfer electrons from the oxidation of organic compounds to carbon dioxide with concomitant extracellular electron transfer toward insoluble acceptors, such as electrode surfaces in microbial fuel cells (MFCs).<sup>1,2</sup> The capability to conduit extracellular electron transfer and the natural abundance of *Geobacter* species in distinct environments opened routes to the development of *Geobacter*-based biotechnological applications, which include bioremediation, bioenergy, and biofuel production.<sup>3</sup>

MFCs are devices that use bacterial metabolism to produce an electrical current from a wide range of organic substrates. These devices are composed by cathodic and anodic compartments separated by a proton/cation exchange membrane. In the latter compartment, the anode serves as extracellular electron acceptor.<sup>1,4-6</sup> Electrons collected on the anode are transported to the cathode via an external circuit. This direct conversion of organic wastes or renewable biomass to electricity in MFCs constitutes a very promising strategy to produce energy from inexpensive material sources.<sup>1,7-11</sup> Currently, the power output of MFCs is not yet considerable and further research is necessary to optimize energy production.<sup>12</sup> Because one of the key reactions in MFCs is the oxidation of organic matter coupled to electron transfer to the anode, understanding the factors that control the activity of microbes that colonize electrodes and,

therefore, the extracellular electron transfer mechanisms is important.

Several genetic studies have shown the involvement of different cytochromes in the electron transfer to extracellular acceptors.<sup>13-18</sup> However, these mechanisms are still poorly understood, particularly in the *Geobacteraceae* family. It is nowadays consensual that these electron routes include multiple redox proteins to ensure an efficient electron transfer from the cytoplasm to the outer cell surface. Among these, the periplasmic cytochromes warrant particular attention as they constitute a crucial interface for electron transfer between inner and outer membrane components. A family of five periplasmic triheme cytochromes (designated PpcA-E) was identified in the bacterium *Geobacter sulfurreducens*.<sup>19</sup> Genetic studies using *G. sulfurreducens* cells with genes coding for these cytochromes knocked-out showed that the reduction rates of extracellular acceptors are affected.<sup>20</sup> The redox properties of these cytochromes have been characterized in detail, with the exception of PpcC.<sup>21,22</sup> In the particular case of PpcA, the most abundant periplasmic cytochrome in *G. sulfurreducens*<sup>23,24</sup> and the most likely electron carrier destined to the outer surface,<sup>25</sup> it was shown that the redox potentials of the three heme groups are modulated by the pH providing the protein the

**Received:** August 5, 2014

**Revised:** October 2, 2014

**Published:** October 2, 2014

necessary thermodynamic properties to couple  $e^-/H^+$  transfer in the pH range from 6.5 to 8.5.<sup>22,26</sup> This feature might represent additional mechanisms contributing to the  $H^+$  electrochemical gradient across the periplasmic membrane that drives ATP synthesis and probably explains why *G. sulfurreducens* cells become metabolically inactive at pH 6 or lower.<sup>27–30</sup> The global redox potential values of PpcA are centered at  $-117\text{ mV}$  (pH 6.5) and  $-148\text{ mV}$  (pH 8.5).<sup>26</sup> This potential window is well framed in the Nernstian response around  $-150\text{ mV}$  measured on *G. sulfurreducens* biofilms grown on electrode surfaces.<sup>6,25,31</sup>

One strategy that can be explored to increase the current production in MFCs is the adaptation of the growth rates of *G. sulfurreducens* cultures to higher ionic strength. This would lower the internal resistance of MFCs and, concomitantly, increase the current production.<sup>32</sup> However, the ionic strength can alter the redox properties of proteins, affecting their functional mechanisms and preventing the survival of the bacterium. Because *in situ* measurements of the apparent redox potential values in *G. sulfurreducens* biofilms are closely related with those observed for PpcA, in this work we investigated the effect of the ionic strength on the redox properties and functional mechanism of this protein. The results obtained provide for the first time a clear illustration of the functional robustness of PpcA at high ionic strength and are discussed in the context of MFCs optimization.

## MATERIALS AND METHODS

**Bacterial Growth and Purification of PpcA.** The expression and purification of PpcA was carried out as previously described.<sup>19,33</sup> Briefly, *Escherichia coli* strain BL21(DE3) cells containing the plasmid pEC86<sup>34</sup> were transformed with the plasmid pCK32 containing PpcA gene and grown on 2xYT culture medium. After reaching an  $OD_{600}$  of  $\sim 1.5$ , cultures were processed in either of two ways: (a) addition of  $10\text{ }\mu\text{M}$  isopropyl  $\beta$ -D-thiogalactoside (IPTG) and overnight incubation at  $30^\circ\text{C}$  to express unlabeled protein, followed by cell harvesting by centrifugation; (b) cell collection by centrifugation, washing twice with 250 mL of M9 medium, resuspending in minimal media (in a ratio of 250 mL of minimal medium for each liter of 2xYT medium) supplied with 1 g/L  $^{15}\text{NH}_4\text{Cl}$  as the nitrogen source, 1 mM of the heme precursor  $\alpha$ -aminolevulinic acid, trace amounts of metal ion salts, biotin, and thiamine, to express  $^{15}\text{N}$ -labeled protein. Cells were then incubated overnight at  $30^\circ\text{C}$  in the presence of 0.8 mM IPTG and harvested by centrifugation. The cytochrome PpcA was purified by cation exchange and gel filtration. The purity of the proteins was evaluated by SDS-PAGE (15%), stained with Coomassie blue.

**NMR Studies. Preparation of NMR Samples.** For NMR experiments, samples were lyophilized and dissolved in a NaCl/phosphate buffer solution to the desired final ionic strength value.  $^{15}\text{N}$  labeled samples were prepared in 92%  $\text{H}_2\text{O}/8\%$   $^{2}\text{H}_2\text{O}$ . Unlabeled samples were prepared in 92%  $\text{H}_2\text{O}/8\%$   $^{2}\text{H}_2\text{O}$  or in  $^{2}\text{H}_2\text{O}$  (99.9 at. %). 1D- $^1\text{H}$  NMR spectra were recorded before and after the lyophilization step to confirm protein integrity. The protein concentrations were  $300\text{ }\mu\text{M}$ , 1 mM, and  $70\text{ }\mu\text{M}$  for the NMR experiments acquired in fully reduced, fully oxidized, and partially oxidized samples, respectively. The reduced sample was obtained by adding gaseous hydrogen in the presence of catalytic amounts of Fe-hydrogenase isolated from *Desulfovibrio vulgaris* (Hildenborough), as previously described.<sup>35</sup> Partially oxidized samples were obtained by removing the hydrogen from a fully reduced sample with argon, followed by the addition of controlled amounts of air into the NMR tube with a Hamilton syringe. The pH of the fully reduced and partially oxidized

samples was adjusted inside an anaerobic glove chamber with argon circulation to avoid sample reoxidation.

**NMR Experiments.** All the NMR experiments were performed at 288 K on a Bruker Avance 600 spectrometer equipped with a triple-resonance cryoprobe (TCI).  $^1\text{H}$  chemical shifts were calibrated using the water signal as internal reference and the  $^{15}\text{N}$  and  $^{13}\text{C}$  chemical shifts were calibrated through indirect referencing.<sup>36</sup> The NMR spectra were processed using TOPSPIN (BrukerBiospin, Karlsruhe, Germany).

**NMR Experiments in the Reduced form.** To monitor the effect of the ionic strength on the heme core and global protein fold, 2D-NMR spectra were recorded at 0.02, 0.10, 0.25, 0.50, and 1.00 M (final ionic strength value) and pH 8.0. The following spectra were acquired: 2D- $^1\text{H}$ -COSY, 2D- $^1\text{H}$ -TOCSY (40 and 80 ms mixing time) and 2D- $^1\text{H}$ -NOESY (50 and 100 ms mixing time), for unlabeled sample. All 2D-NMR spectra were recorded by collecting  $4096\text{ }(t_2) \times 256\text{ }(t_1)$  data points to cover a sweep width of 8 kHz.

**NMR Experiments in the Oxidized form.** The following spectra were acquired for the unlabeled sample in 92%  $\text{H}_2\text{O}/8\%$   $^{2}\text{H}_2\text{O}$ : 2D- $^1\text{H}$ -COSY, 2D- $^1\text{H}$ -TOCSY (45 ms mixing time) and 2D- $^1\text{H}$ -NOESY (80 ms mixing time) at pH 7.1. These 2D-NMR spectra were acquired with a sweep width of 24 kHz in both dimensions. For the  $^{15}\text{N}$  labeled sample a series of 2D- $^1\text{H}$ ,  $^{15}\text{N}$ -HSQC NMR spectra was acquired with a sweep width of 24 kHz in  $F_2$  and 39 kHz in  $F_1$ . These spectra were used to monitor the chemical shift perturbation caused by the ionic strength on PpcA backbone NH signals. The weighted average chemical shift ( $\Delta\delta_{\text{avg}}$ ) of each NH signal was calculated as

$$\Delta\delta_{\text{comb},j} = \sqrt{(\Delta\delta_{\text{H}})^2 + (w_i\Delta\delta_{\text{N}})^2}$$

where  $\Delta\delta_{\text{H}}$  is the chemical shift change in ppm in  $^1\text{H}$  dimension,  $\Delta\delta_{\text{N}}$  is the chemical shift change in ppm in  $^{15}\text{N}$  dimension, and the term  $w_i = |\gamma^{15}\text{N}|/|\gamma^1\text{H}|$  compensates for the scaling differences between  $^{15}\text{N}$  and  $^1\text{H}$  chemical shifts.<sup>37</sup> The cutoff value was determined by an iterative procedure to calculate the correct standard deviation to zero value ( $\sigma_0^{\text{corr}}$ ), as described by Schumann and co-workers.<sup>37</sup>

**NMR Redox Titrations.** To monitor the stepwise oxidation of the individual hemes at each ionic strength, 2D- $^1\text{H}$ -exchange spectroscopy (EXSY) NMR spectra were acquired in the pH range 5.5–9 for partially oxidized samples, as previously described.<sup>22</sup> The spectra were acquired by collecting  $2048\text{ }(t_2) \times 256\text{ }(t_1)$  data points to cover a sweep width of 30 kHz.

**Assignment of the NMR Signals.** The PpcA NH, except for the first two residues, and heme substituents NMR signals were previously assigned at 0.10 M ionic strength (pH 7.1 and 298 K).<sup>38</sup> Because temperature affects the chemical shift of the NMR signals, in particular in the oxidized form, the same set of NMR experiments was acquired at 288 K in the present work. These experiments were then used to assign the NH and heme signals at 288 K using the methodologies previously described.<sup>39</sup> The program Sparky - NMR Assignment and Integration Software<sup>40</sup> was used for 2D-NMR spectra inspection and for assignment of the signals.

**Redox Titrations Followed by Visible Spectroscopy.** Due to the low reduction potentials of the heme groups, the redox titrations of cytochrome PpcA were carried out inside an anaerobic chamber (MBraun) at 288 K, as described previously.<sup>35</sup> PpcA samples with  $18\text{ }\mu\text{M}$  protein concentration were prepared at pH 7.0 and 8.0 in NaCl/phosphate buffer solution at different ionic strength values. To check for hysteresis,

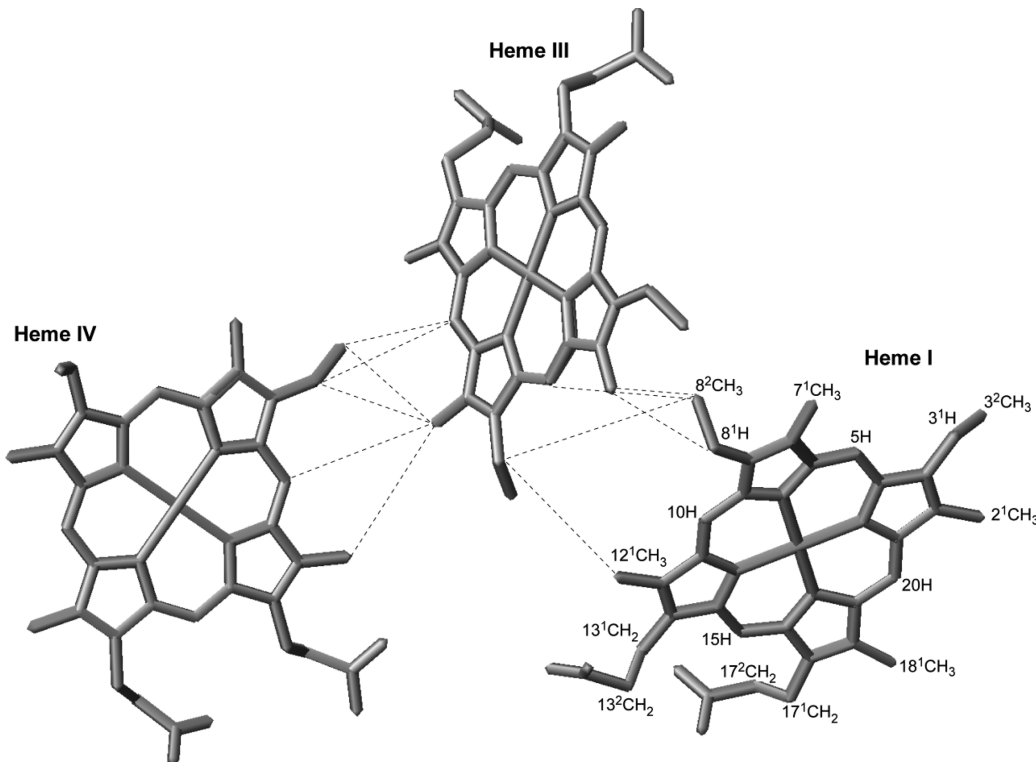


**Figure 1.** Heme core architecture of PpcA (PDB code, 2LDO<sup>39</sup>). The interheme NOE connectivities observed in the <sup>1</sup>H-NOESY spectra (100 ms mixing time) obtained at the different ionic strength are illustrated by the dashed lines. The hemes are numbered I, III, and IV, a designation that derives from the superimposition of the hemes in cytochromes *c*<sub>7</sub> with those of the structurally homologous tetrahemcytobromes *c*<sub>3</sub>. The IUPAC nomenclature for tetrapyrroles is illustrated in heme I.<sup>49</sup>

each redox titration was performed in both oxidative and reductive directions. The reduced fraction of the proteins was determined by integrating the area of the  $\alpha$ -peak (552 nm) above the line connecting the flanking isosbestic points (543 and 559 nm) to subtract the optical contribution of the redox mediators, as previously described.<sup>35</sup> The experiments were performed at least two times, and the reduction potentials (relative to standard hydrogen electrode, SHE) were found to be reproducible within  $\pm 5$  mV.

**Probing the Individual Heme Oxidation Profiles and Determination of Their Thermodynamic Properties.** A thermodynamic model was previously used to determine the redox properties of PpcA heme redox centers at 0.25 M.<sup>22,26</sup> Therefore, the same model was used in the present work to characterize in detail the thermodynamic properties of PpcA over the ionic strength range from 0.02 to 1.00 M. The theoretical framework of the model was previously described by Morgado and co-workers<sup>22,26</sup> and can be summarized as follows. In solution, a triheme cytochrome displays three consecutive reversible steps of one-electron transfer that convert the fully reduced state (stage 0, S<sub>0</sub>) to the fully oxidized state (stage 3, S<sub>3</sub>). Therefore, four different redox stages can be defined, each consisting of microstates with the same number of oxidized hemes. A supplementary figure is provided to illustrate the different redox stages and respective microstates (Figure S1, Supporting Information). Taking as reference the fully reduced and protonated protein, the energy of the microstates can be described in the full range of pH and solution potential as sums of 10 parameters: the three energies of oxidation of the hemes (reduction potentials) and the pK<sub>a</sub> of the redox-Bohr center plus six two-center interaction energies (three heme–heme and

three redox-Bohr). In experimental terms, 2D-<sup>1</sup>H EXSY NMR experiments can be used to monitor the stepwise oxidation of each heme by following the chemical shifts of a single heme methyl throughout the different oxidation stages, as the interconversion between oxidation microstates within the same oxidation stage (intramolecular electron exchange) is fast and the interconversion between microstates belonging to different oxidation stages (intermolecular electron exchange) is slow on the NMR time scale.<sup>41,42</sup> To obtain the absolute values for the 10 thermodynamic parameters, the NMR information needs to be complemented with visible redox titration data obtained at least at two different pH values (for a review see ref 43). In the previous characterization of PpcA at 0.25 M ionic strength the chemical shifts obtained for the heme methyls 12<sup>1</sup>CH<sub>3</sub><sup>I</sup>, 7<sup>1</sup>CH<sub>3</sub><sup>III</sup>, and 12<sup>1</sup>CH<sub>3</sub><sup>IV</sup> (labeled according to the IUPAC nomenclature, Figure 1) in each oxidation stage were fitted simultaneously with visible redox titrations data obtained at pH 7 and 8.<sup>22</sup> To obtain the thermodynamic parameters of PpcA, at the different ionic strength values, the same set of heme methyls was used and the visible redox titrations were performed in identical experimental conditions.

## RESULTS

**Impact of the Ionic Strength on PpcA Global Fold and Heme Core Structure.** The triheme cytochrome PpcA contains only 71 residues, and thus the heme proton signals are excellent probes to detect any structural rearrangement within the heme core. Therefore, we probed the impact of the ionic strength on the PpcA heme core architecture by comparing the chemical shifts of the heme proton NMR signals at 288 K and different ionic strength values. These signals were assigned as

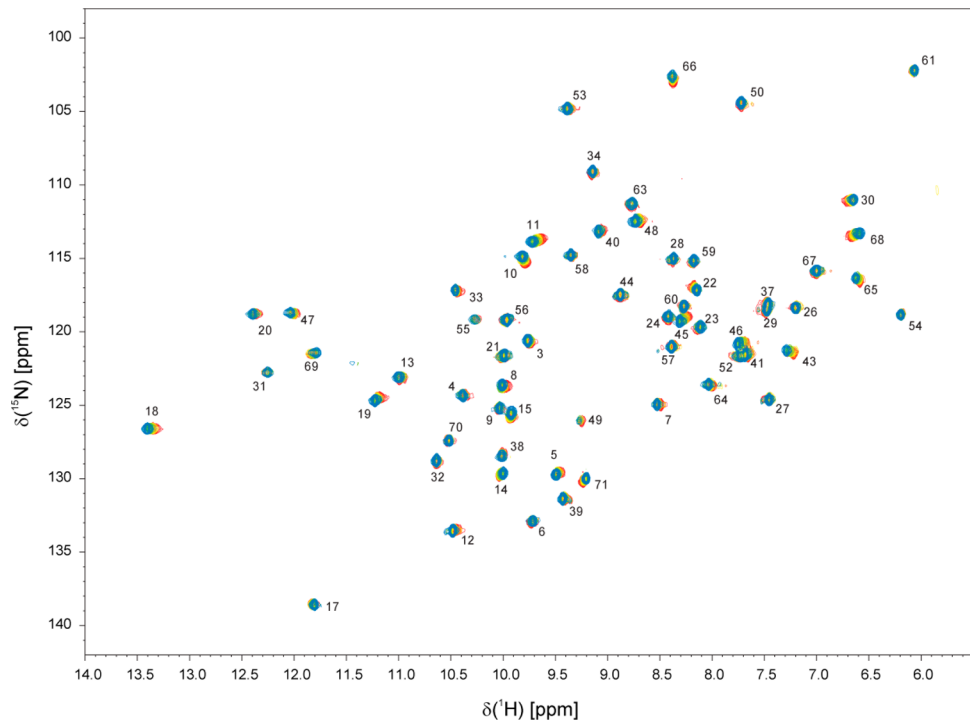


**Figure 2.** Overlay of the 2D-<sup>1</sup>H,<sup>15</sup>N HSQC NMR spectra of <sup>15</sup>N-enriched PpcA (1 mM) at different ionic strength in the oxidized state (288 K and pH 7.1). The contours of the signals are shown in blue (0.02 M), green (0.10 M), yellow (0.25 M), orange (0.50 M), and red (1.00 M). The assignments of NH signals are indicated.

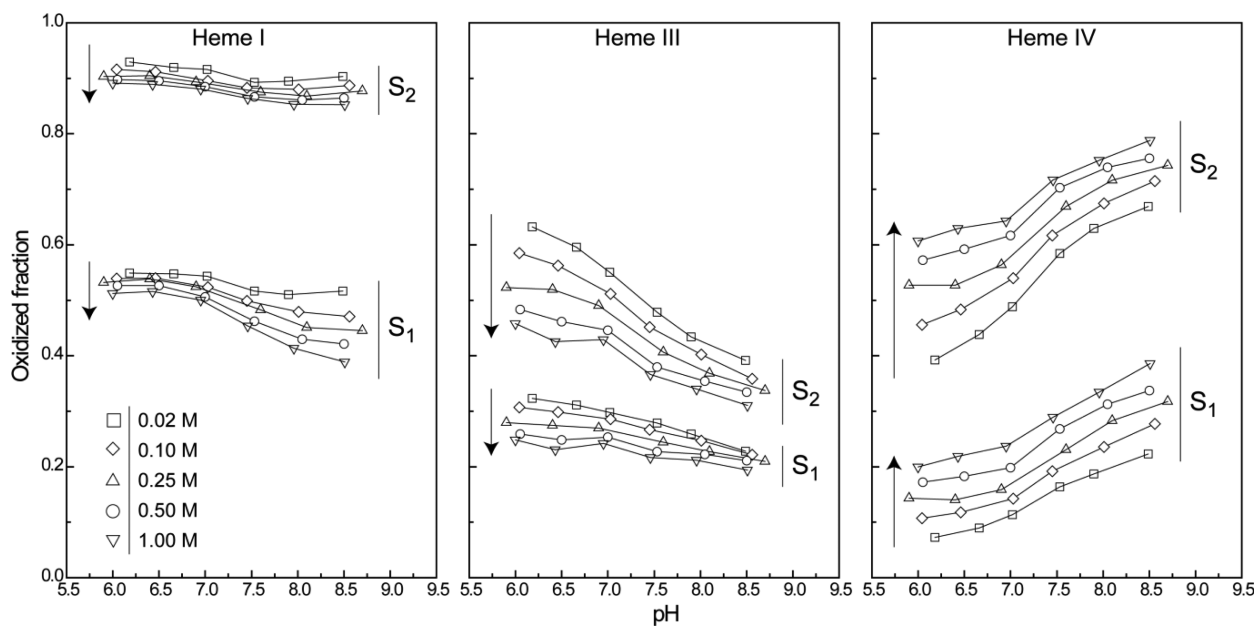


**Figure 3.** Oxidized fraction of PpcA heme groups in oxidation stages 1 ( $S_1$ ) and 2 ( $S_2$ ) at different pH and ionic strength values: □, 0.02 M; ◇, 0.10 M; △, 0.25 M; ○, 0.50 M; ▽, 1.00 M. The heme oxidation fractions, in each stage of oxidation were calculated according to the equation  $x_i = (\delta_i - \delta_0)/(\delta_3 - \delta_0)$ , where  $\delta_i$ ,  $\delta_0$ , and  $\delta_3$  are the observed chemical shift of the heme methyl in oxidation stage  $i$ , 0, and 3, respectively. By definition, the oxidation fraction values at oxidation stages  $S_0$  and  $S_3$  are 0 and 1, respectively. For clarity these values are not represented in the figure. The arrows show the increase of the ionic strength.

described previously<sup>35</sup> and their chemical shift values are provided in the Supporting Information (Table S1). The rmsd values between the chemical shifts observed at low (0.02 M) and high (1.00 M) ionic strength are small (0.02 for all the hemes), indicating that the heme core of PpcA is unaffected. In addition, the same set of NOE connectivities between the heme groups

were observed at all ionic strength values, further confirming that the heme core arrangement is conserved (Figure 1).

After probing the impact of the ionic strength on the heme core architecture, we then investigated this effect on the global structure of the protein. The chemical shift perturbation measurements on PpcA backbone NH signals were monitored

by recording a series of 2D-<sup>1</sup>H,<sup>15</sup>N HSQC NMR spectra (Figure 2). The comparison of these spectra shows a similar dispersion of the signals indicating that, in addition to the heme core, the overall fold of the protein is also maintained over the ionic strength 0.02–1.00 M range.

**Impact of the Ionic Strength on the Heme Oxidation Profiles of Cytochrome PpcA.** Having established that the heme core and global fold of the protein are unaffected by the ionic strength, we then evaluated the influence of this parameter on the oxidation profile of each heme group. The heme oxidation fractions were determined from the chemical shifts of the heme methyls <sup>12</sup><sup>1</sup>CH<sub>3</sub><sup>I</sup>, <sup>7</sup><sup>1</sup>CH<sub>3</sub><sup>III</sup>, and <sup>12</sup><sup>1</sup>CH<sub>3</sub><sup>IV</sup> measured in the different oxidation stages from 2D-<sup>1</sup>H EXSY NMR spectra acquired at the different ionic strength values, in the pH range from 5.5 to 9. Examples of these spectra are given in Figure S2 (Supporting Information). Figure 3 depicts the variation of the heme oxidation fractions at intermediate oxidation stages (S<sub>1</sub> and S<sub>2</sub>). Analysis of this figure shows that the heme oxidation profiles are affected by the ionic strength and by the solution pH. The effect of the pH on the heme oxidation fraction profiles is essentially the same in the entire ionic strength range. This effect was previously discussed in detail at the ionic strength value of 0.25 M<sup>22</sup> and, for this reason, it is not addressed in detail in the present work.

**Effect of the Ionic Strength on the Heme Redox Properties and on the Functional Mechanism of PpcA at Physiological pH.** To determine the impact of the ionic strength on the heme oxidation profiles and redox properties, we then moved to the detailed thermodynamic characterization of PpcA at the different ionic strength values. This was achieved by fitting for each ionic strength, the pH dependence of the chemical shift of the heme methyls <sup>12</sup><sup>1</sup>CH<sub>3</sub><sup>I</sup>, <sup>7</sup><sup>1</sup>CH<sub>3</sub><sup>III</sup>, and <sup>12</sup><sup>1</sup>CH<sub>3</sub><sup>IV</sup>, measured in the different stages of oxidation, together with data from visible redox titrations obtained at pH 7 and 8, within the framework of the thermodynamic model described in the Materials and Methods. The thermodynamic parameters obtained from the fitting are indicated in Table 1. The quality of the fittings obtained for the pH dependence of the NMR paramagnetic chemical shifts clearly shows that the experimental data are well described by the model (solid lines in Figure S3, Supporting Information). To evaluate the effect of the ionic strength on the heme redox properties at physiological pH, the oxidation curves of each heme and the molar fraction of each microstate were computed from the thermodynamic parameters listed in Table 1 and are indicated in Figure 4. To better visualize this effect, the heme midpoint reduction potentials are represented as a function of the square root of ionic strength in Figure 5, as previously described for the tetraheme cytochrome c<sub>3</sub> from *Desulfovibrio vulgaris* (Miyazaki).<sup>44</sup>

**NMR Chemical Shift Perturbation Studies at Different Ionic Strength.** The analysis of a series of 2D-<sup>1</sup>H,<sup>15</sup>N HSQC NMR spectra, obtained at different ionic strengths, showed that the most affected NH signals corresponded to Asn<sup>10</sup>, Gly<sup>11</sup>, Lys<sup>18</sup>, Ala<sup>19</sup>, and Cys<sup>30</sup> and those placed in the polypeptide segments Lys<sup>43</sup>-Gly<sup>48</sup> and Cys<sup>65</sup>-Lys<sup>71</sup> (Figure 6). These residues are highlighted on the three-dimensional structure of PpcA (Figure 7).

## DISCUSSION

**Thermodynamic Characterization.** The detailed thermodynamic characterization of PpcA, the most abundant periplasmic cytochrome in *G. sulfurreducens*, at 0.25 M ionic strength showed that the redox potentials of the hemes are

**Table 1. Effect of the Ionic Strength on the Thermodynamic Parameters of PpcA<sup>a</sup>**

	energy (meV)			
	heme I	heme III	heme IV	redox-Bohr center
<b><i>I</i> = 0.02 M</b>				
heme I	<b>-154 (6)</b>	27 (3)	16 (4)	-38 (5)
heme III		<b>-141 (5)</b>	41 (3)	-30 (5)
heme IV			<b>-114 (6)</b>	-63 (4)
redox-Bohr center				<b>495 (9)</b>
<b><i>I</i> = 0.10 M</b>				
heme I	<b>-154 (5)</b>	28 (3)	17 (3)	-36 (5)
heme III		<b>-140 (5)</b>	42 (3)	-31 (5)
heme IV			<b>-120 (6)</b>	-62 (4)
redox-Bohr center				<b>497 (9)</b>
<b><i>I</i> = 0.25 M</b>				
heme I	<b>-154 (5)</b>	27 (2)	16 (3)	-32 (4)
heme III		<b>-138 (5)</b>	41 (3)	-31 (4)
heme IV			<b>-125 (5)</b>	-58 (4)
redox-Bohr center				<b>495 (8)</b>
<b><i>I</i> = 0.50 M</b>				
heme I	<b>-152 (5)</b>	28 (2)	17 (3)	-32 (4)
heme III		<b>-134 (5)</b>	41 (3)	-34 (4)
heme IV			<b>-128 (5)</b>	-57 (4)
redox-Bohr center				<b>490 (8)</b>
<b><i>I</i> = 1.00 M</b>				
heme I	<b>-152 (4)</b>	26 (2)	16 (3)	-28 (4)
heme III		<b>-133 (5)</b>	40 (3)	-32 (4)
heme IV			<b>-132 (5)</b>	-55 (4)
redox-Bohr center				<b>494 (8)</b>

<sup>a</sup>Diagonal values (in bold) correspond to oxidation energies of the hemes and deprotonating energy of the redox-Bohr center. Off-diagonal values are the redox (heme–heme) and redox-Bohr (heme–proton) interaction energies. All energies are reported in meV, with standard errors given in parentheses. For comparison the values previously obtained at 0.25 M<sup>22</sup> are indicated.

modulated by redox and redox-Bohr interactions.<sup>22</sup> This redox network confers to the protein the necessary properties to couple e<sup>-</sup>/H<sup>+</sup> transfer in the physiological pH range for *G. sulfurreducens* growth.<sup>22,26</sup> In the present work, we analyzed the effect of ionic strength on the functional properties of PpcA, using NMR and potentiometric methods. The analysis of the interheme NOE connectivities and chemical shift perturbation measurements on the heme protons and backbone NH signals showed that the heme core and the overall fold of PpcA was unaffected by the ionic strength. This warrants that the changes observed in the redox behavior of the heme groups are independent from any significant structural rearrangement in the protein folding. The heme group whose oxidation profile is the most affected is clearly heme IV, followed by hemes III and I (Figure 3). The effect of the ionic strength on the heme IV oxidation profile is opposite to that observed for the other two hemes. In fact, at any pH value, the oxidation fraction values of heme IV, at both intermediate oxidation stages, increase with increasing ionic strength, in contrast to those of hemes I and III (arrows in Figure 3). This differentiated behavior is not unexpected for a multiheme cytochrome because the total number of oxidized hemes in each oxidation stage is fixed, i.e., one heme in oxidation stage S<sub>1</sub> and

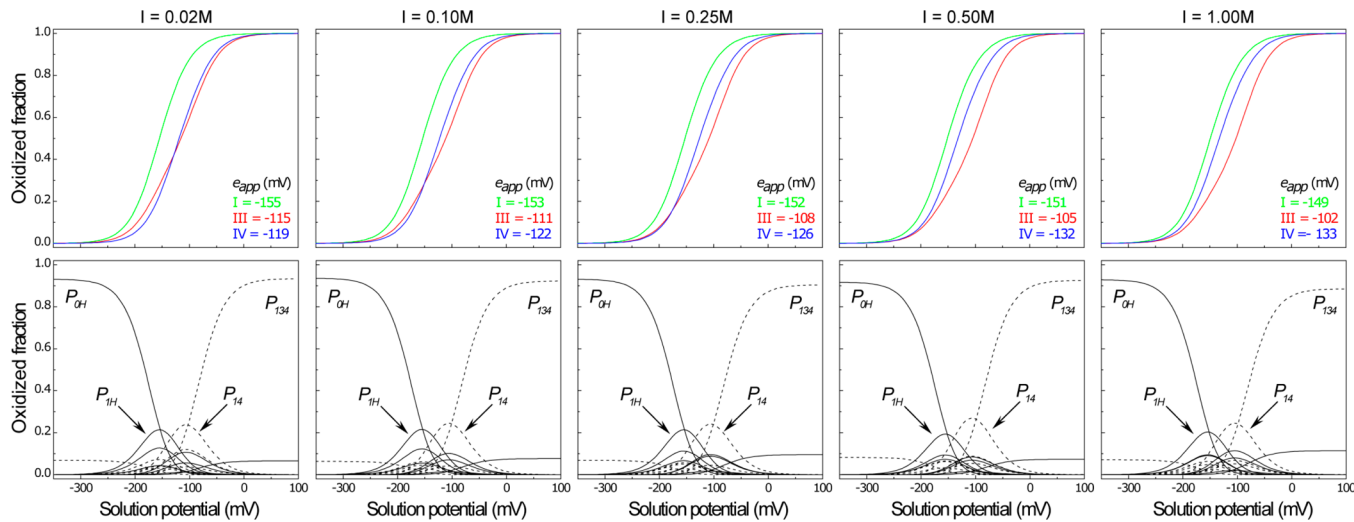


**Figure 4.** Oxidized fractions of the individual hemes (upper panels) and molar fractions of the 16 individual microstates (lower panels) for PpcA at different ionic strengths and pH 7.5. The curves were calculated as a function of the solution reduction potential using the parameters listed in Table 1. In the upper panels the heme  $e_{app}$  values (heme I, green; heme III, red; heme IV, blue) are indicated. In the lower panels solid and dashed lines indicate the protonated and deprotonated microstates, respectively (as described in Figure S1, Supporting Information). For clarity only the relevant microstates are labeled.

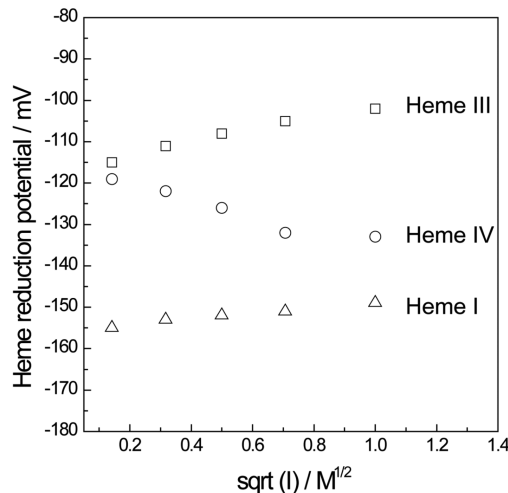


**Figure 5.** Midpoint reduction potential of PpcA heme groups as a function of the square root of the ionic strength at pH 7.5. Triangles, squares, and circles represent hemes I, III, and IV, respectively.

two in oxidation stage  $S_2$  (Figure S1, Supporting Information; see also Materials and Methods). Thus, if one heme becomes more oxidized in a particular oxidation stage, at least one of the other hemes is necessarily more reduced. From the analysis of Figure 3, it is clear that heme I shows the higher oxidation fraction values in oxidation stage  $S_1$  at any pH or ionic strength and therefore dominates the first oxidation step, which connects stages  $S_0$  and  $S_1$  (Figure S1, Supporting Information). The second oxidation step (between stages  $S_1$  and  $S_2$ ) is not dominated by the oxidation of any particular heme group. On the other hand, the last oxidation step (between stages  $S_2$  and  $S_3$ ) at low ionic strength is dominated by the oxidation of heme IV, in the pH range from 6 to 7 and by the oxidation of heme III at higher pH (cf. squares in Figure 3 for hemes III and IV in oxidation stage  $S_2$ ). Notably, as the ionic strength increases, the oxidation of heme III becomes clearly dominant in the last oxidation step in the entire range of pH (cf. inverted triangles in Figure 3 for hemes III and IV in oxidation  $S_2$ ). Previous work undertaken on

PpcA mutated proteins have shown that the order of oxidation of the hemes, particularly when heme III is the last to oxidize, is crucial to establish preferred  $e^-/H^+$  transfer pathways, a key feature of PpcA functional mechanism.<sup>45–47</sup> Therefore, the results obtained at high ionic strength indicate that the increase of this parameter favors the key features of PpcA functional mechanism even at lower pH values.

The detailed thermodynamic characterization of cytochrome PpcA at the different ionic strength values (Table 1) shows that the interactions among the redox centers are subject to small modifications, in agreement with the arguments in literature that for nonsurface groups, such as the hemes, the presence of counterions should have a small effect on pairwise charge–charge interactions between redox centers in a protein.<sup>48</sup> For each ionic strength value, the smallest redox interactions are established between the hemes that are structurally further apart, hemes I and IV. The strongest redox-Bohr interactions are observed for heme IV. The positive values of the redox interactions indicate that the oxidation of a particular heme renders the oxidation of its neighbors more difficult, which is expected on an electrostatic basis. Similarly, the negative redox-Bohr interactions (between the hemes and the redox-Bohr center) indicate that the oxidation of the hemes facilitates the deprotonation of the redox-Bohr center and vice versa. The redox-Bohr center in PpcA was previously assigned to heme IV propionate  $P_{13}$ .<sup>22,35,39</sup> The higher redox-Bohr interaction observed for heme IV over the fully ionic strength range (Table 1) indicates that the redox-Bohr center remains associated with this heme.

The reduction potential of heme IV is the most affected in the fully reduced and protonated protein (−18 mV) and decreases with increasing ionic strength (Table 1). Although to a smaller extent, the reduction potential of heme III is also affected but increases with the ionic strength (+8 mV). On the other hand, the reduction potential of heme I is essentially unaffected by the ionic strength (+2 mV). However, as discussed above, the heme midpoint reduction potentials ( $e_{app}$ , i.e., the point at which the oxidized and reduced fractions of each heme are equally populated) are modulated by redox interaction networks

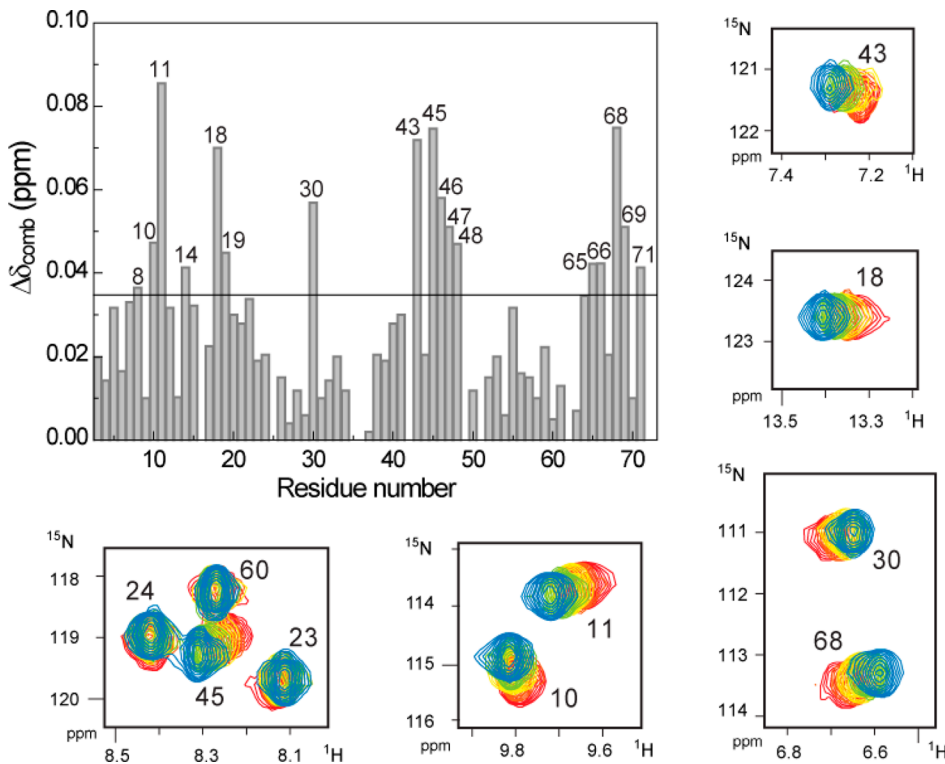


**Figure 6.** Combined chemical shift changes determined from the directly observed <sup>1</sup>H and <sup>15</sup>N chemical shifts in the 2D-<sup>1</sup>H,<sup>15</sup>N HSQC NMR spectra. The chemical shift changes were calculated from the spectra acquired at 0.02 and 1.00 M (Figure 2). The horizontal line in the inset was determined with the standard deviation to zero value,  $\sigma_0^{\text{corr}}$  (Materials and Methods). Expansions indicate the spectral regions of the spectra containing the NH signals with the largest chemical shift perturbation (Gly<sup>11</sup>, Lys<sup>18</sup>, Lys<sup>43</sup>, Met<sup>45</sup>, Cys<sup>68</sup>). The contours of the signals are shown in blue (0.02 M), green (0.10 M), yellow (0.25 M), orange (0.50 M), and red (1.00 M).

determined by the oxidation state of neighboring hemes (redox interactions) and by the solution pH (redox-Bohr interactions). From the analysis of the individual heme oxidation curves it is clear that the  $e_{\text{app}}$  values of heme IV decrease with increasing ionic strength, also at physiological pH (Figures 4 and 5), and its oxidation stands out at earlier oxidation stages compared to the case for heme III. As a consequence, the positive redox interaction between hemes IV and III has a larger contribution in the midpoint reduction potential of the latter, which increases proportionally to the increase of heme IV oxidation fraction at earlier stages of oxidation. As a result, the last step of oxidation is even more dominated by the oxidation of heme III and the order of oxidation of the hemes in PpcA is thus I–IV–III, in the entire range of ionic strength (Figure 4, upper panels and Figure 5). As discussed above, this order of oxidation of the hemes is crucial to establish the preferred  $e^-/H^+$  transfer pathway, which is a key feature of the PpcA functional mechanism.<sup>45–47</sup> Therefore, to evaluate the effect of the ionic strength on PpcA functional mechanism, the relative contribution of each of the 16 possible microstates was determined as a function of the solution potential at each ionic strength value. Such study was previously undertaken at 0.25 M, and a coherent electron transfer pathway coupled to proton transfer was identified.<sup>22</sup> The relative variation of the PpcA microstates is depicted in Figure 4 (lower panels) together with those obtained in the present work for the other ionic strength values. The results obtained showed that despite the changes observed in the heme oxidation profiles, the protein is still able to perform a concerted  $e^-/H^+$  transfer between oxidation stages 1 and 2. In fact, in the entire range of ionic strength the oxidation stage 0 is dominated by the fully reduced and protonated microstate  $P_{0\text{H}}$  and stage 1 is dominated by the

oxidation of heme I ( $P_{1\text{H}}$ ) while keeping the redox-Bohr center protonated. Oxidation stage 2 is dominated by the oxidation of hemes I and IV and deprotonation of the acid–base center ( $P_{14}$ ), that remains deprotonated in stage 3 upon full oxidation of heme III ( $P_{134}$ ). Therefore, a route is defined for electron transfer in PpcA:  $P_{0\text{H}} \rightarrow P_{1\text{H}} \rightarrow P_{14} \rightarrow P_{134}$ . Taking these observations together, it is clear that despite the decrease of  $e_{\text{app}}$  of heme IV with increasing ionic strength, PpcA retains the essential features of its functional mechanism.

**Structural Correlations.** The thermodynamic characterization of PpcA over the ionic strength range from 0.02 to 1.00 M within the physiological pH values for *G. sulfurreducens* cellular growth indicated that (i) the reduction potential of heme IV decreases with increasing ionic strength, (ii) the reduction of heme III increases with increasing ionic strength, and (iii) the cytochrome is designed to ensure a concerted  $e^-/H^+$  transfer also at high ionic strength. The chemical shift perturbation studies performed at the different ionic strength values clearly showed that the two polypeptide segments that contain the higher number of affected residues are located on the surface of the PpcA molecule in polypeptide regions that enwrap heme IV (Figure 7). The solution structure of PpcA shows the presence of eight lysine residues around heme IV (Lys<sup>7</sup>, Lys<sup>9</sup>, Lys<sup>14</sup>, Lys<sup>43</sup>, Lys<sup>52</sup>, Lys<sup>64</sup>, Lys<sup>70</sup>, Lys<sup>71</sup>) that confer a highly positively charged surface near this heme.<sup>39</sup> Therefore, as a consequence of the high positive electrostatic surface around heme IV it is expected that the exposed side chains of lysine residues will be more shielded by their counterions as the ionic strength of the solution increases. This explains the observed decrease in the electron affinity by heme IV (i.e., lower reduction potentials) with increasing ionic strength. Although in much lower number, some

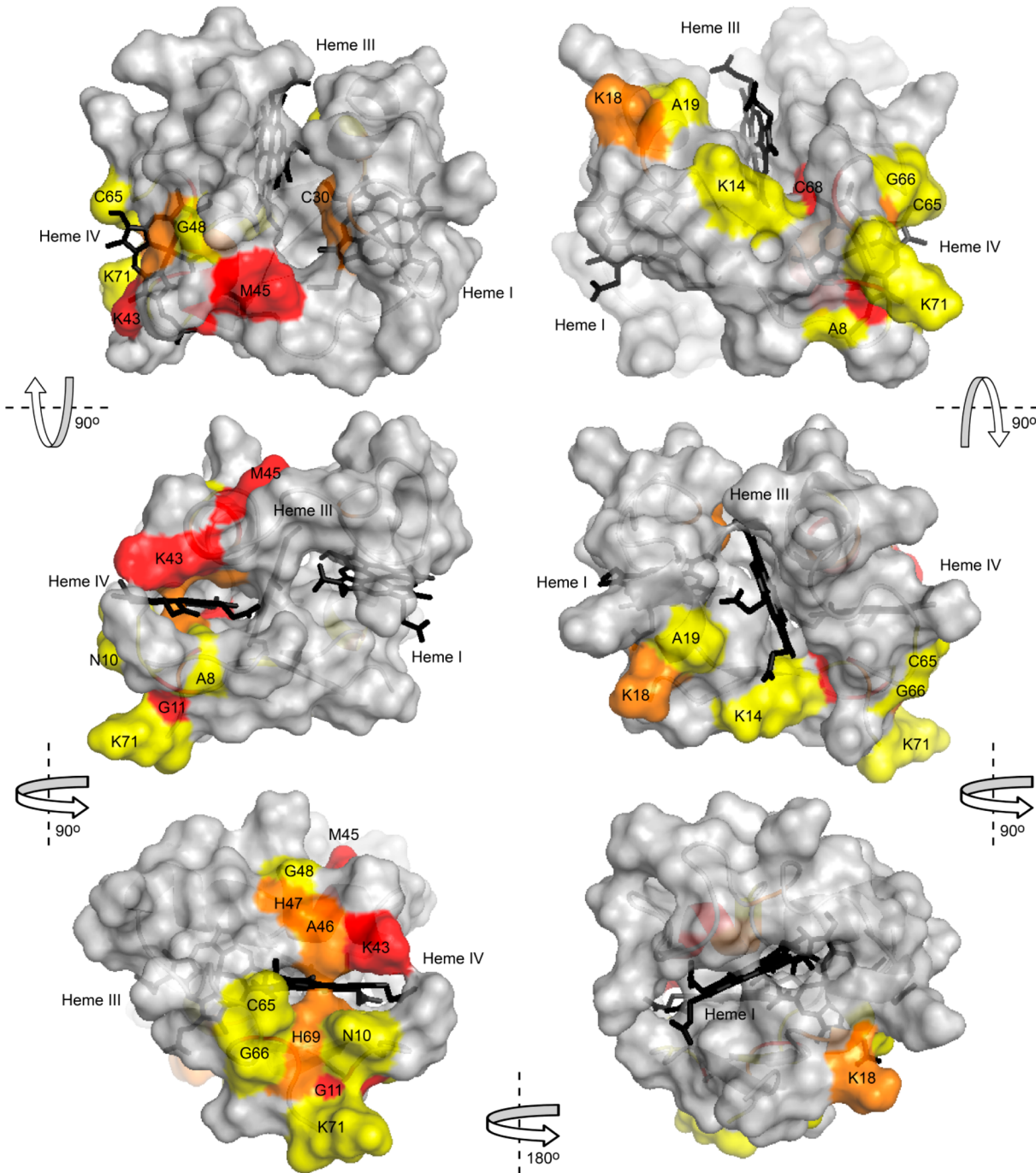


**Figure 7.** Surface map of significantly perturbed residues in PpcA with ionic strength. The molecular surface was generated in PyMOL by using the PpcA structure (PDB code, 2LDO<sup>39</sup>). Residues for which the amide resonances experienced small ( $\Delta\delta_{\text{comb}} > 0.035$  ppm), medium ( $\Delta\delta_{\text{comb}} \geq 0.05$  ppm), and large ( $\Delta\delta_{\text{comb}} \geq 0.07$  ppm) shifts are colored yellow, orange, and red, respectively. The hemes are shown in black. The left and right panels are related by a 180° rotation. Upper images are related to lower images by 90° rotations as indicated.

residues placed in the vicinity of heme III were also affected by the increase of ionic strength (Figure 7). This probably results in small variations on local dielectric constants in the heme environment, which might also contribute to the observed increase in the reduction potential of heme III.

## CONCLUSIONS

In the present work we studied the effect of the ionic strength on the redox properties of the periplasmic triheme cytochrome PpcA from *G. sulfurreducens*. The results showed that the

individual heme oxidation profiles of heme IV are the most affected. The observed changes result in the decrease of the reduction potential of heme IV with the increase of ionic strength. As a consequence, the difference between the reduction potential of heme III and its predecessor in the heme oxidation order I–IV–III is increased at high ionic strength, maintaining the preferential electron  $e^-/H^+$  transfer pathway in PpcA.<sup>45,47</sup> The perturbations on the NMR signals corresponding to the PpcA backbone NH showed that the region around heme IV is more affected by the ionic strength and provided a structural rational for the modification of the redox properties of this

cytochrome. The location of several lysine residues around heme IV confers a highly positively electrostatic surface near this heme, which is therefore the most affected by ionic interactions. The shielding of lysine positively charged side chain by the counterions stabilizes the oxidized form of the heme group and explains the decrease in the reduction potential of heme IV. Overall, the effect of the ionic strength on the functional properties described here for cytochrome PpcA from *G. sulfurreducens* correlates with the structural data available and provides an excellent example of how a periplasmic protein is designed to maintain the key features of its functional mechanism in the presence of abiotic physical-chemical parameter changes. The functional robustness showed by PpcA suggests that the growth rates of the electrogenic *G. sulfurreducens* cultures can be adapted, within the proper limits for bacterial growth, to higher ionic strengths. This will reduce the internal resistance of the MFCs, leading to a sizable increase in the current production.

## ASSOCIATED CONTENT

### Supporting Information

Supplementary table with chemical shifts of PpcA heme protons in the reduced state at different ionic strength values (Table S1). Supplementary figures with electronic distribution for the different microstates in triheme cytochromes (Figure S1), examples of 2D-<sup>1</sup>H EXSY NMR spectra obtained at intermediate oxidation stages (Figure S2), and fitting of the thermodynamic model to the experimental data at different ionic strength values (Figure S3). This material is available free of charge via the Internet at <http://pubs.acs.org>.

## AUTHOR INFORMATION

### Corresponding Author

\*C. A. Salgueiro. E-mail: csalgueiro@fct.unl.pt

### Author Contributions

<sup>†</sup>These authors contributed equally to the work.

### Notes

The authors declare no competing financial interest.

## ACKNOWLEDGMENTS

We acknowledge Professor D. L. Turner for the thermodynamic model software used in the present work. This work was supported by project grant PTDC/BBB-BEP/0753/2012 (to C.A.S.) and the strategic grant PEst-C/EQB/LA0006/2013 (to REQUIMTE Laboratório Associado) from Fundação para a Ciência e a Tecnologia (FCT), Portugal. The NMR spectrometers used are part of The National NMR Facility, supported by Fundação para a Ciência e a Tecnologia (RECI/BBB-BQB/0230/2012). J.M.D. is the recipient of grant SFRH/BD/89701/2012 from FCT.

## REFERENCES

- Bond, D. R.; Lovley, D. R. Electricity production by *Geobacter sulfurreducens* attached to electrodes. *Appl. Environ. Microbiol.* **2003**, *69*, 1548–1555.
- Bond, D. R.; Holmes, D. E.; Tender, L. M.; Lovley, D. R. Electrode-reducing microorganisms that harvest energy from marine sediments. *Science* **2002**, *295*, 483–485.
- Lovley, D. R.; Ueki, T.; Zhang, T.; Malvankar, N. S.; Shrestha, P. M.; Flanagan, K. A.; Aklujkar, M.; Butler, J. E.; Giloteaux, L.; Rotaru, A. E.; et al. *Geobacter*: The microbe electric's physiology, ecology, and practical applications. *Adv. Microb. Physiol.* **2011**, *59*, 1–100.
- Chang, I. S.; Moon, H.; Bretschger, O.; Jang, J. K.; Park, H. I.; Nealson, K. H.; Kim, B. H. Electrochemically active bacteria (EAB) and mediator-less microbial fuel cells. *J. Microbiol. Biotechnol.* **2006**, *16*, 163–177.
- Holmes, D. E.; Chaudhuri, S. K.; Nevin, K. P.; Mehta, T.; Methé, B. A.; Liu, A.; Ward, J. E.; Woodard, T. L.; Webster, J.; Lovley, D. R. Microarray and genetic analysis of electron transfer to electrodes in *Geobacter sulfurreducens*. *Environ. Microbiol.* **2006**, *8*, 1805–1815.
- Srikanth, S.; Marsili, E.; Flickinger, M. C.; Bond, D. R. Electrochemical characterization of *Geobacter sulfurreducens* cells immobilized on graphite paper electrodes. *Biotechnol. Bioeng.* **2008**, *99*, 1065–1073.
- Logan, B. E.; Regan, J. M. Microbial challenges and applications. *Environ. Sci. Technol.* **2006**, *40*, 5172–5180.
- Lovley, D. R. Bug juice: harvesting electricity with microorganisms. *Nat. Rev. Microbiol.* **2006**, *4*, 497–508.
- Du, Z.; Li, H.; Gu, T. A state of the art review on microbial fuel cells: A promising technology for wastewater treatment and bioenergy. *Biotechnol. Adv.* **2007**, *25*, 464–482.
- Allen, R. M.; Bennetto, H. P. Microbial fuel-cells - electricity production from carbohydrates. *Appl. Biochem. Biotechnol.* **1993**, *39*, 27–40.
- Gil, G. C.; Chang, I. S.; Kim, B. H.; Kim, M.; Jang, J. K.; Park, H. S.; Kim, H. J. Operational parameters affecting the performance of a mediator-less microbial fuel cell. *Biosens. Bioelectron.* **2003**, *18*, 327–334.
- Kim, M.-S.; Lee, Y.-j. Optimization of culture conditions and electricity generation using *Geobacter sulfurreducens* in a dual-chambered microbial fuel-cell. *Int. J. Hydrogen Energy* **2010**, *35*, 13028–13034.
- Qian, X.; Reguera, G.; Mester, T.; Lovley, D. R. Evidence that OmcB and OmpB of *Geobacter sulfurreducens* are outer membrane surface proteins. *FEMS Microbiol. Lett.* **2007**, *277*, 21–27.
- Richter, H.; Nevin, K. P.; Jia, H.; Lowy, D. A.; Lovley, D. R.; Tender, L. M. Cyclic voltammetry of biofilms of wild type and mutant *Geobacter sulfurreducens* on fuel cell anodes indicates possible roles of OmcB, OmcZ, type IV pili, and protons in extracellular electron transfer. *Energy Environ. Sci.* **2009**, *2*, 506–516.
- Rutter, A. J.; Thomas, K. L.; Herbert, D.; Henderson, R. J.; Lloyd, D.; Harwood, J. L. Oxygen induction of a novel fatty acid n-6 desaturase in the soil protozoan, *Acanthamoeba castellanii*. *Biochem. J.* **2002**, *368*, 57–67.
- Mehta, T.; Coppi, M. V.; Childers, S. E.; Lovley, D. R. Outer membrane c-type cytochromes required for Fe(III) and Mn(IV) oxide reduction in *Geobacter sulfurreducens*. *Appl. Environ. Microbiol.* **2005**, *71*, 8634–8641.
- Kim, B. C.; Postier, B. L.; Didonato, R. J.; Chaudhuri, S. K.; Nevin, K. P.; Lovley, D. R. Insights into genes involved in electricity generation in *Geobacter sulfurreducens* via whole genome microarray analysis of the OmcF-deficient mutant. *Bioelectrochemistry* **2008**, *73*, 70–75.
- Mehta, T.; Childers, S. E.; Glaven, R.; Lovley, D. R.; Mester, T. A putative multicopper protein secreted by an atypical type II secretion system involved in the reduction of insoluble electron acceptors in *Geobacter sulfurreducens*. *Microbiology* **2006**, *152*, 2257–2264.
- Pokkuluri, P. R.; Londer, Y. Y.; Duke, N. E.; Long, W. C.; Schiffer, M. Family of cytochrome c<sub>7</sub>-type proteins from *Geobacter sulfurreducens*: structure of one cytochrome c<sub>7</sub> at 1.45 Å resolution. *Biochemistry* **2004**, *43*, 849–859.
- Shelobolina, E. S.; Coppi, M. V.; Korenevsky, A. A.; Didonato, L. N.; Sullivan, S. A.; Konishi, H.; Xu, H.; Leang, C.; Butler, J. E.; Kim, B. C.; Lovley, D. R. Importance of c-type cytochromes for U(VI) reduction by *Geobacter sulfurreducens*. *BMC Microbiol.* **2007**, *7*, 16.
- Morgado, L.; Bruix, M.; Londer, Y. Y.; Pokkuluri, P. R.; Schiffer, M.; Salgueiro, C. A. Redox-linked conformational changes of a multiheme cytochrome from *Geobacter sulfurreducens*. *Biochem. Biophys. Res. Commun.* **2007**, *360*, 194–198.
- Morgado, L.; Bruix, M.; Pessanha, M.; Londer, Y. Y.; Salgueiro, C. A. Thermodynamic characterization of a triheme cytochrome family from *Geobacter sulfurreducens* reveals mechanistic and functional diversity. *Biophys. J.* **2010**, *99*, 293–301.
- Lloyd, J. R.; Leang, C.; Hodges Myerson, A. L.; Coppi, M. V.; Cuifo, S.; Methe, B.; Sandler, S. J.; Lovley, D. R. Biochemical and genetic

- characterization of PpcA, a periplasmic *c*-type cytochrome in *Geobacter sulfurreducens*. *Biochem. J.* **2003**, *369*, 153–161.
- (24) Ding, Y. H.; Hixson, K. K.; Giometti, C. S.; Stanley, A.; Estevez-Núñez, A.; Khare, T.; Tollaksen, S. L.; Zhu, W.; Adkins, J. N.; Lipton, M. S.; et al. The proteome of dissimilatory metal-reducing microorganism *Geobacter sulfurreducens* under various growth conditions. *Biochim. Biophys. Acta* **2006**, *1764*, 1198–1206.
- (25) Liu, Y.; Kim, H.; Franklin, R. R.; Bond, D. R. Linking spectral and electrochemical analysis to monitor *c*-type cytochrome redox status in living *Geobacter sulfurreducens* biofilms. *Chemphyschem.* **2011**, *12*, 2235–2241.
- (26) Morgado, L.; Dantas, J. M.; Bruix, M.; Londer, Y. Y.; Salgueiro, C. A. Fine tuning of redox networks on multiheme cytochromes from *Geobacter sulfurreducens* drives physiological electron/proton energy transduction. *Bioinorg. Chem. Appl.* **2012**, *2012*, 1–9.
- (27) Babauta, J. T.; Nguyen, H. D.; Harrington, T. D.; Renslow, R.; Beyenal, H. pH, redox potential and local biofilm potential microenvironments within *Geobacter sulfurreducens* biofilms and their roles in electron transfer. *Biotechnol. Bioeng.* **2012**, *109*, 2651–2662.
- (28) Franks, A. E.; Nevin, K. P.; Jia, H.; Izallalen, M.; Woodard, T. L.; Lovley, D. R. Novel strategy for three-dimensional real-time imaging of microbial fuel cell communities: monitoring the inhibitory effects of proton accumulation within the anode biofilm. *Energy Environ. Sci.* **2009**, *2*, 113–119.
- (29) Torres, C. I.; Kato Marcus, A.; Rittmann, B. E. Proton transport inside the biofilm limits electrical current generation by anode-respiring bacteria. *Biotechnol. Bioeng.* **2008**, *100*, 872–881.
- (30) Torres, C. I.; Lee, H. S.; Rittmann, B. E. Carbonate species as OH<sup>−</sup> carriers for decreasing the pH gradient between cathode and anode in biological fuel cells. *Environ. Sci. Technol.* **2008**, *42*, 8773–8777.
- (31) Marsili, E.; Rollefson, J. B.; Baron, D. B.; Hozalski, R. M.; Bond, D. R. Microbial biofilm voltammetry: direct electrochemical characterization of catalytic electrode-attached biofilms. *Appl. Environ. Microbiol.* **2008**, *74*, 7329–7337.
- (32) Liu, H.; Cheng, S.; Logan, B. E. Power generation in fed-batch microbial fuel cells as a function of ionic strength, temperature, and reactor configuration. *Environ. Sci. Technol.* **2005**, *39*, 5488–5493.
- (33) Fernandes, A. P.; Couto, I.; Morgado, L.; Londer, Y. Y.; Salgueiro, C. A. Isotopic labeling of *c*-type multiheme cytochromes overexpressed in *E. coli*. *Prot. Expr. Purif.* **2008**, *59*, 182–188.
- (34) Arslan, E.; Schulz, H.; Zufferey, R.; Kunzler, P.; Thöny-Meyer, L. Overproduction of the *Bradyrhizobium japonicum* *c*-type cytochrome subunits of the *cbb*<sub>3</sub> oxidase in *Escherichia coli*. *Biochem. Biophys. Res. Commun.* **1998**, *251*, 744–747.
- (35) Morgado, L.; Bruix, M.; Orshonsky, V.; Londer, Y. Y.; Duke, N. E.; Yang, X.; Pokkuluri, P. R.; Schiffer, M.; Salgueiro, C. A. Structural insights into the modulation of the redox properties of two *Geobacter sulfurreducens* homologous triheme cytochromes. *Biochim. Biophys. Acta* **2008**, *1777*, 1157–1165.
- (36) Wishart, D. S.; Bigam, C. G.; Yao, J.; Abildgaard, F.; Dyson, H. J.; Oldfield, E.; Markley, J. L.; Sykes, B. D. <sup>1</sup>H, <sup>13</sup>C and <sup>15</sup>N chemical shift referencing in biomolecular NMR. *J. Biomol. NMR* **1995**, *6*, 135–140.
- (37) Schumann, F. H.; Riepl, H.; Maurer, T.; Gronwald, W.; Neidig, K. P.; Kalbitzer, H. R. Combined chemical shift changes and amino acid specific chemical shift mapping of protein-protein interactions. *J. Biomol. NMR* **2007**, *39*, 275–289.
- (38) Dantas, J. M.; Morgado, L.; Catarino, T.; Kokhan, O.; Raj Pokkuluri, P.; Salgueiro, C. A. Evidence for interaction between the triheme cytochrome PpcA from *Geobacter sulfurreducens* and anthrahydroquinone-2,6-disulfonate, an analog of the redox active components of humic substances. *Biochim. Biophys. Acta* **2014**, *1837*, 750–760.
- (39) Morgado, L.; Paixao, V. B.; Schiffer, M.; Pokkuluri, P. R.; Bruix, M.; Salgueiro, C. A. Revealing the structural origin of the redox-Bohr effect: the first solution structure of a cytochrome from *Geobacter sulfurreducens*. *Biochem. J.* **2012**, *441*, 179–187.
- (40) Goddard, T. D.; Kneller, D. G. University of California, San Francisco, USA, 2007.
- (41) Salgueiro, C. A.; Turner, D. L.; Santos, H.; LeGall, J.; Xavier, A. V. Assignment of the redox potentials to the four haems in *Desulfovibrio vulgaris* cytochrome *c*<sub>3</sub> by 2D-NMR. *FEBS Lett.* **1992**, *314*, 155–158.
- (42) Santos, H.; Moura, J. J.; Moura, I.; LeGall, J.; Xavier, A. V. NMR studies of electron transfer mechanisms in a protein with interacting redox centres: *Desulfovibrio gigas* cytochrome *c*<sub>3</sub>. *Eur. J. Biochem.* **1984**, *141*, 283–296.
- (43) Turner, D. L.; Salgueiro, C. A.; Catarino, T.; LeGall, J.; Xavier, A. V. NMR studies of cooperativity in the tetrahaem cytochrome *c*<sub>3</sub> from *Desulfovibrio vulgaris*. *Eur. J. Biochem.* **1996**, *241*, 723–731.
- (44) Ohmura, T.; Nakamura, H.; Niki, K.; Cusanovich, M. A.; Akutsu, H. Ionic strength-dependent physicochemical factors in cytochrome *c*<sub>3</sub> regulating the electron transfer rate. *Biophys. J.* **1998**, *75*, 1483–1490.
- (45) Morgado, L.; Dantas, J. M.; Simoes, T.; Londer, Y. Y.; Pokkuluri, P. R.; Salgueiro, C. A. Role of Met(58) in the regulation of electron/proton transfer in trihaem cytochrome PpcA from *Geobacter sulfurreducens*. *Biosci. Rep.* **2013**, *33*, 11–22.
- (46) Dantas, J. M.; Morgado, L.; Londer, Y. Y.; Fernandes, A. P.; Louro, R. O.; Pokkuluri, P. R.; Schiffer, M.; Salgueiro, C. A. Pivotal role of the strictly conserved aromatic residue F15 in the cytochrome *c*<sub>7</sub> family. *J. Biol. Inorg. Chem.* **2012**, *17*, 11–24.
- (47) Morgado, L.; Lourenço, S.; Londer, Y. Y.; Schiffer, M.; Pokkuluri, P. R.; Salgueiro, C. Dissecting the functional role of key residues in triheme cytochrome PpcA: a path to rational design of *G. sulfurreducens* strains with enhanced electron transfer capabilities. *PLoS One.* **2014**, *9*, e105566.
- (48) Louro, R. O.; Catarino, T.; Paquete, C. M.; Turner, D. L. Distance dependence of interactions between charged centres in proteins with common structural features. *FEBS Lett.* **2004**, *576*, 77–80.
- (49) Moss, G. P. Nomenclature of tetrapyrroles. Recommendations 1986 IUPAC-IUB joint commission on biochemical nomenclature (JCBN). *Eur. J. Biochem.* **1988**, *178*, 277–328.